PHYSICAL REVIEW C VOLUME 23, NUMBER 5 MAY 1981

Cross sections relevant to gamma-ray astronomy: Proton induced reactions

P. Dyer
Nuclear Physics Laboratory, University of Washington, Seattle, Washington 98195
*and Heavy Ion Laboratory, Michigan State University, East Lansing, Michigan 48824**

D. Bodansky, A. G. Seamster, and E. B. Norman
Nuclear Physics Laboratory, University of Washington, Seattle, Washington 98195

D. R. Maxson
Department of Physics, Brown University, Providence, Rhode Island 02912
(Received 2 June 1980)

Gamma-ray production cross sections have been measured for the gamma-ray lines most strongly excited in the proton bombardment of ^{12}C, ^{14}N, ^{16}O, ^{20}Ne, ^{24}Mg, ^{28}Si, and ^{56}Fe, for proton energies from threshold to 23 MeV. In addition, cross sections for the $^{14}N(p,n)^{14}O$ and $^{56}Fe(p,n)^{56}Co$ reactions were determined from delayed gamma-ray yields. Ge(Li) detectors were used. Tabulations of cross sections averaged over proton energy bins of 1 MeV and over power law distributions in proton energy are provided for calculations relevant to gamma-ray line astronomy. Examples are given of astrophysical information which might be extracted from spectra acquired with gamma-ray spectrometers in space, using these cross sections, e.g., parameters describing the energy distribution of incident protons.

[NUCLEAR REACTIONS $p+^{12}C$, ^{14}N, ^{16}O, ^{20}Ne, ^{24}Mg, ^{28}Si, ^{56}Fe; $^{14}N(p,n)$, $^{56}Fe(p,n)$. E = threshold to 23 MeV. Measured γ production cross sections. Applications to γ line astronomy.]

I. INTRODUCTION

The range of the astronomically observed electromagnetic spectrum has been extended in the last two decades to the gamma-ray region, and observations of nuclear gamma-ray lines have begun in the last decade. This new field of observational astronomy is in a period of rapid development as large, high-resolution germanium detectors are being put into space. Extensive reviews of the progress and possibilities in this area have been presented by Ramaty and collaborators[1-3] and by Chupp.[4] Accordingly, here we only briefly summarize the main features of gamma-ray line astronomy.

Gamma-ray lines provide a unique probe of the universe, as their presence is a signature of specific nuclear reactions taking place in astrophysical environments. Moreover, because of the high penetrability of gamma rays through matter, it may be possible to learn about processes such as star formation in interstellar clouds not penetrated by electromagnetic radiation from atomic or molecular line emission. Spectra of observed gamma rays can in principle be analyzed to obtain relative abundances of isotopes and energy spectra of accelerated particles at astrophysical sites. Shapes of the gamma-ray lines may provide information on the directions of accelerated particles and distinguish between gaseous matter and grains.

Possible sites of discrete gamma-ray production include solar flares, interstellar gas and dust, regions of star formation, novae, supernovae, neutron stars, and black holes. At such sites gamma rays may be produced by several distinct mechanisms. Radioactive products of nucleosynthesis from objects such as novae and supernovae can emit gamma rays. Neutron capture and positron annihilation can also produce discrete gamma rays of 2.22 and 0.511 MeV. In this work we are primarily interested in gamma rays from a further mechanism: charged particle induced nuclear reactions.

When protons and alpha particles in an astrophysical environment are accelerated to energies of a few MeV or greater, collisions with nuclei in the ambient medium can produce gamma rays when a nuclear reaction leaves the product in an excited state. An example is the reaction $^{12}C(p,p')^{12}C(4.44\ \text{MeV})$, which results in emission of a 4.44-MeV gamma ray. This same gamma-ray transition can also be excited by ^{12}C ions incident upon ambient hydrogen; the line seen in astronomical observations will have greater Doppler broadening than that for incident protons.

A review of the observational status of gamma-ray astronomy has been given by Chupp.[4] As yet, there have been relatively few clear-cut identifications of gamma-ray lines from charged particle induced nuclear reactions. The best evidence exists for the 4.44-MeV line from ^{12}C, which has been reported in observations of solar flares,[5] the galactic center,[6] and Centaurus A,[7] although

 © 1981 The American Physical Society

some of these identifications are not completely unambiguous. The remainder of the paper is predicated on the assumption that further observations may lead to more extensive spectra of gamma rays from nuclear reactions.

In order to extract quantities such as the relative nuclear abundances and the energy spectra of the interacting particles from observed gamma-ray spectra, it is necessary to know cross sections for the production of gamma rays in proton and alpha-particle induced reactions over a broad range of incident energies. Ramaty *et al.*,[1] have recently made a compilation of such cross sections, based on gamma-ray branching ratios, inelastic proton scattering cross sections, and a few measured gamma-ray production cross sections. The required input from measured quantities, however, was by no means complete.

In the present work, gamma-ray production cross sections have been measured for lines which are expected to be prominent by virtue of high target abundances and high cross sections. In particular, we have measured cross sections for the production of gamma rays from ^{12}C, ^{14}N, ^{16}O, ^{20}Ne, ^{24}Mg, ^{28}Si, and ^{56}Fe nuclei, for protons from threshold energies up to about 23 MeV and for alpha particles from threshold to about 27 MeV. Only the proton cross sections are reported in this paper; the alpha-particle cross sections and the analysis of Doppler-broadened line shapes will be reported later.

The experimental technique used for measuring gamma-ray production cross sections is described in Sec. II. Contributions from delayed activities, particularly from the $^{14}N(p,n)\,^{14}O$ and $^{56}Fe(p,n)\,^{56}Co$ reactions, are considered in Sec. III. The gamma-ray cross section results are presented in Sec. IV. The discussion, in Sec. V, includes comments on astrophysical relevance.

II. EXPERIMENTAL METHOD

A. General arrangement

Solid or gas targets were bombarded by beams of protons from the University of Washington three-stage tandem Van de Graaff accelerator, and gamma rays in the range from 0.8 to 12 MeV were detected in two Ge(Li) detectors. The targets were mounted in a thin-walled aluminum hemispherical chamber of 20-cm radius. A Si(Li) particle detector was also mounted inside the chamber; particle spectra were accumulated for each run, but were used only for trouble shooting purposes. A typical beam current was 10 nA. The beam energy resolution was a few keV. After passing through the target, the beam was integrated in a Faraday cup.

B. Gamma-ray detection system

The two Ge(Li) detectors were mounted on carts which traveled along a circular rail. The front faces of the Ge(Li) crystals were 21 cm from the target. The beam collimators, chamber, and Ge(Li) support table were aligned by telescope prior to each data accumulation period, and the alignment was checked at the end of each period. The isotropy of the system was checked before and after each data accumulation period by measuring the angular distribution of gamma rays from a ^{54}Mn source placed at the position of the target.

One Ge(Li) detector was 47 mm in diameter and 54 mm in length, with a nominal efficiency of 15.3% (relative to that of a 7.5 cm × 7.5 cm NaI (Tl) crystal for 1.33-MeV gamma rays at 25 cm); the other was 42 mm in diameter and 39 mm in length, with a nominal efficiency of 9.6%. [A small amount of $p + {}^{56}Fe$ data was acquired with a smaller Ge(Li) detector; these data were normalized to that taken with the larger detectors.] Lead absorbers of thickness 0.9 or 1.7 mm were placed in front of the detectors to reduce the count rate from x rays and low-energy gamma rays.

Energy spectra were accumulated with an SDS 930 computer. Detector resolution was a few keV, and count rates above about 100 keV were usually a few thousand per second. In order to determine the dead time of the system, the digital output of the current integrator was fed alternately into the triggers of two pulsers connected to the preamplifiers of the two detectors. Sample spectra are shown in Fig. 1.

C. Measurement of Ge(Li) detector efficiencies

The Ge(Li) detector efficiencies were determined by a combination of source and reaction techniques. Sources were placed at the center of the scattering chamber used for the cross-section measurements. Relative efficiencies from 0.8 to 3.3 MeV were determined with a ^{56}Co source. Absolute efficiencies in this range were determined with a set of sources calibrated in strength to 3%: ^{54}Mn (0.835 MeV), ^{22}Na (1.275 MeV), and ^{60}Co (1.332 MeV).

Efficiencies for the 4.44- and 6.13-MeV gamma rays were determined by simultaneously measuring gamma-ray yields (in the standard geometry) and yields of inelastically scattered protons for the $^{12}C(p,p')\,^{12}C$ (4.44 MeV) reaction at 12.0 MeV and for the $^{16}O(p,p')\,^{16}O$ (6.13 MeV) reaction at 9.2 MeV. At these energies, the only significant channels for producing gamma rays are inelastic scattering to the indicated levels.

The simultaneous measurements eliminated tar-

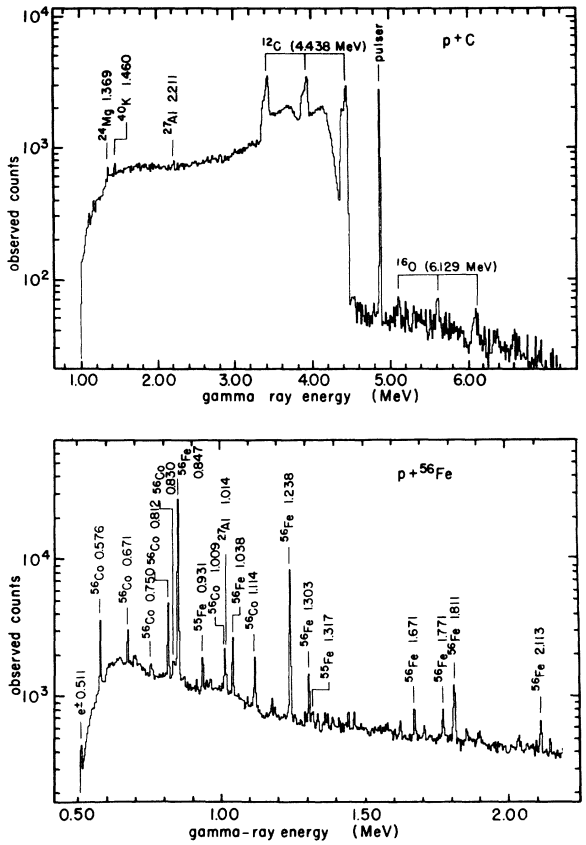

FIG. 1. Observed gamma-ray spectra at $E_p = 15$ MeV: top—carbon target; bottom—iron target. Vertical lines are located at energies corresponding to gamma-ray emission energies (in MeV), uncorrected for Doppler shifts arising from motion of the excited nucleus. For the ^{12}C and ^{16}O gamma rays, the photopeak and the single and double escape peaks are separately indicated. For the C spectrum, contaminant lines are indicated which arise from oxygen in the target, room background, and proton interactions in the aluminum walls of the scattering chamber.

get thickness and beam current integration uncertainties. To compare the proton and gamma-ray yields it was necessary to determine the yields integrated over all angles. The gamma-ray angular distribution was explicitly determined by measuring the yields at several angles and fitting them with a series of Legendre polynomials (even order through 4 for ^{12}C and through 6 for ^{16}O; see Sec. II E). The proton detector was held fixed at a single angle during these measurements (at 60° for the carbon case and at 30° or 72° for the oxygen case), and the angle-integrated proton yield was inferred from proton angular distributions established in separate measurements.

These proton angular distributions were determined in a standard way, using two Si(Li) detectors, one to map out the angular distribution from 10° to 170° and the other to serve as a monitor. This was done in a larger (1.52 m diameter) scattering chamber than that used for the gamma-ray measurements. The uncertainty in the extrapolation to 0° and to 180° was estimated to be about 1% of the integrated yield.

A 1.8-mg/cm^2 carbon target was used for the $^{12}C(p,p')\,^{12}C$ measurement. The $^{16}O(p,p')\,^{16}O$ measurement was more difficult because of the closeness of the peaks from the 6.05- and 6.13-MeV states. Data forward of 100° were acquired with a 0.5-mg/cm^2-thick Mylar target. Measurements backward of 100° (which required use of a reflection geometry) were made with a 0.13-mg/cm^2-thick SiO_2 target. Protons from ^{28}Si inelastic scattering did not interfere with the ^{16}O groups of interest in this angular range.

D. Targets

Target thicknesses and target angles were chosen in a compromise between the desire to map out excitation functions quickly and the desire to avoid significant gaps or loss of structure in the excitation functions. The targets used and their thicknesses are listed in Table I.

Thicknesses of the solid targets were measured from the energy loss of alpha particles from an ^{241}Am source plus one or more of the following techniques: Coulomb scattering, measurements of yields of scattered particles using known cross sections,[8] and comparison of gamma yields with those of gaseous targets. For each target we measured the uniformity over a 0.6-cm diameter area with collimated alpha particles from the ^{241}Am source. Oxygen contents were determined by measuring elastically scattered 16-MeV protons at 80°, using the measured cross sections of Daehnick,[9] and carbon contents were measured by comparisons to a carbon target. The resulting impurity corrections were small (less than 5% by weight), except for the silicon targets, which had 32% oxygen, by weight.

Nitrogen, oxygen, and neon data were acquired with gas targets. The gas cell was 2.54 cm in outside diameter, with a 0.083-cm-thick stainless steel wall, beam entrance and exit apertures covered with 1.8-mg/cm^2-thick nickel foils, and an aperture at 90° for particle monitoring. Gases were high purity, natural gases.

Gas pressure was regulated with a Cartesian manostat. The increase in length of the gas cell due to the bowing of the foils under pressure was measured with an optical comparator, and a 1.6% correction to the target thicknesses was made. The uncertainty in the thicknesses was about 5%,

TABLE I. Targets used for gamma-ray cross section measurements. The indicated thickness is the stopping power thickness, as seen by the beam, and includes isotopic and elemental impurities (corrected for stopping power differences).

Target nucleus	Target composition	Thickness (mg/cm^2)	Target angle	Beam energy range (MeV)
Solid targets				
^{12}C	natural	1.8 ± 0.1	15°	5.1–23.0
^{24}Mg	isotopic, >99% [a]	0.23 ± 0.03	60°	2.2–2.8
		2.2 ± 0.1	30°	2.8–12.0
		3.2 ± 0.15	30°	12.0–13.5
		3.2 ± 0.15	60°	13.5–16.8
		2.2 ± 0.1	60°	16.8–24.0
^{28}Si	natural	0.54 ± 0.03	10°	2.8–5.0
		0.90 ± 0.05		
		1.7 ± 0.06	10°	5.0–12.0
		1.7 ± 0.06	40°	12.0–23.0
^{56}Fe	isotopic, >99% [b]	3.1 ± 0.3	20°, 45°	4.0–13.4
		3.1 ± 0.3	10°	13.4–23.0
Gaseous targets				
^{14}N	natural	0.79 ± 0.04		3.7–4.4
		1.5 ± 0.07		4.4–6.1
		2.5 ± 0.1		6.1–23.0
^{16}O	natural	2.9 ± 0.14		7.1–23.0
^{20}Ne	natural	0.54 ± 0.03		2.3–3.1
		1.6 ± 0.08		3.1–24.0

[a] Verified by comparing yields of 1.612- and 1.809-MeV gamma rays from natural and isotopic targets, using the $p+^{25}Mg$ and $p+^{26}Mg$ reactions, respectively.

[b] Verified by comparing yields of 1.408-MeV gamma rays from natural and isotopic targets, using the $\alpha+^{54}Fe$ reaction.

arising primarily from the lack of a gas temperature measurement. We assumed that the gas temperature was within 10 °K of room temperature, giving a 3.4% uncertainty in the target thickness. Typical beam currents were under 10 nA.

E. Data acquisition and analysis

At the beginning of each data accumulation period, and usually at the end, the efficiencies of the Ge(Li) detectors and the isotropy of the system were measured with the radioactive sources. For the cross section measurements, data accumulation times were typically 10 min. Beam energies were stepped in units of average energy loss in the target up to about 14 MeV, after which larger steps were taken, when the cross section was no longer rapidly varying. Complete gamma-ray angular distributions were measured occasionally. Other checks included integrating the beam current over the chamber as well as the Faraday cup (no difference was ever detected), and measurements of backgrounds with no target, with an empty gas cell, or with the beam off. Overlapping data points were acquired when changes in the experimental configuration were made. During two periods, we measured cross sections at one or more energies on all targets, in order to compare measurements made under experimental conditions as nearly identical as possible. The 4.44- and 6.13-MeV Ge(Li) efficiency measurements were made during these same two periods.

The cross sections were derived from photopeak yields, with the exception of the 6.13-MeV gamma-ray line from ^{16}O, where the double escape peak from the 7.12-MeV gamma-ray line overlapped the 6.13-MeV photopeak, and therefore the cross section was found from the double escape peak. The primary concern was to treat the gamma-ray yield extraction and background subtraction for the data runs in the same way as for the efficiency measurements. With the exception of the 4.44-MeV gamma-ray peaks from ^{12}C, background subtraction was based on a simple average of the background above and below the peak.

In the case of the 4.44-MeV gamma rays, the line shape for the photopeak was quite broad, especially for the higher energy incident protons. Thus the low energy part of the "peak" included the rising Compton edge from events Doppler-shifted to higher energies. To correct for this, a channel-by-channel analysis of the background was made, treating the observed peak as a sum

of (essentially monoenergetic) individual peaks, each with its own Compton tail. The basic line shape at a single energy was deduced by a study of narrow lines produced at low incident proton energy. Both photopeak and double escape peak yields were extracted. The resulting two cross sections typically agreed to within 1.5%. We quote only the photopeak results because the continuous background is lower in the photopeak region and therefore the photopeak results have smaller statistical errors than the double escape results, and may have smaller systematic errors as well.

In the case of 1.37-MeV gamma rays produced in the ^{24}Mg(p,p') ^{24}Mg reaction, a small (not more than 3%) correction was applied to the yields, as these gamma rays may also be produced in the ^{27}Al(p,α) ^{24}Mg reaction, when scattered beam hits the walls of the chamber or beam pipe. This correction was found using the yields of 1.01-MeV gamma rays from the ^{27}Al(p,p') ^{27}Al reaction (in the Mg target runs) and the ratio of the yields for wall-produced 1.37- and 1.01-MeV gamma rays, as determined in runs with a carbon target. It was similarly found that 0.844-MeV gamma rays from the ^{27}Al(p,p') ^{27}Al reaction made a contribution of (5 ± 3)% to the extracted yields for 0.847-MeV gamma rays from the ^{56}Fe(p,p') ^{56}Fe reaction, and a 5% correction was applied to these cross sections.

The angular distribution of gamma rays with respect to the beam direction is given by

$$W(\theta)=\sum_{l=0}^{l=l_{\max}} a_l P_l(\cos\theta) \quad (l \text{ even}), \tag{1}$$

where $l_{\max}$ is the smaller of the following two quantities: (1) twice the spin of the decaying state, and (2) twice the multipolarity of the gamma ray.[10] With the exception of the 6.13-MeV gamma rays from ^{16}O, the gamma rays considered in this work have a multipolarity of 2 or less, so that $l_{\max}$ is 4 or less, and there are at most three terms ($l=0,2,4$) in the above expansion. Since the total cross section is proportional to a_0, only this coefficient needs to be determined. We have thus placed two detectors at angles for which $P_4(\cos\theta)$ is zero, 30.6° and 109.9°, and determined a_0 and the total cross section from measurements at these two angles.

In the case of the $E3$, 6.13-MeV gamma rays from ^{16}O, there are four terms in the angular distribution, so that at least three points on the angular distribution are required to obtain the total cross section. In this case we determined the complete angular distribution by making measurements at four angles (26°, 48.8°, 90°, and 104°).

There are two corrections to the total cross sections extracted from yields at 30.6° and 109.9° that we did not make, but that we have determined to be small. The first correction would be required if the beam spot was not at the center of the circle along which the detectors traveled. Isotropy measurements with a ^{54}Mn source placed at the center of the chamber indicated that the errors introduced in the cross sections were usually less than 1%, and in a few extreme cases might have been as high as 4%. The second correction arises from the lab-to-center-of-mass transformation. Neglect of this correction leads to errors of 1% for the worst case of 23 MeV $p+^{12}$C and less error elsewhere (with one detector at 30.6° and one at 109.9°, effects for the two detectors largely cancel).

Complete angular distributions were measured at intervals of about 2 MeV in beam energy for the carbon and oxygen targets and at one or two energies for other targets. These distributions were fit with the appropriate Legendre polynomial expansions, and total cross sections were extracted; these cross sections were in good agreement with those extracted from measurements at two angles (or four in the case of 6.13-MeV gamma rays), the largest percentage difference being 4%. No asymmetry about 90° was observed. Sample angular distributions are shown in Fig. 2. (These data have not been corrected for the finite size of the detectors; such a correction does not affect the extraction of total cross sections, as the finite-detector attenuation factor for the $l=0$ term is unity.[11])

F. Special normalization for the 4.44-MeV line from ^{12}C

The 4.44-MeV gamma-ray excitation function measurements were made in two partially overlapping series of runs, using a multilayer target, 1.8 mg/cm^2 thick. The target thickness was determined by using an alpha-source thickness gauge, by comparison of yields with those from a thinner but more uniform carbon foil, by comparisons of yields with those from a gas target (CH_4), and by comparisons to presumably known cross sections for inelastic and elastic proton scattering on carbon.[12] The results of these determinations spanned a range of about ±10%, representing a dispersion larger than the presumed uncertainties in the individual measurements. Furthermore, the alpha-source studies showed that the target was not of uniform thickness, presumably due to a physical flaw in one or more of the foils of which the target was comprised.

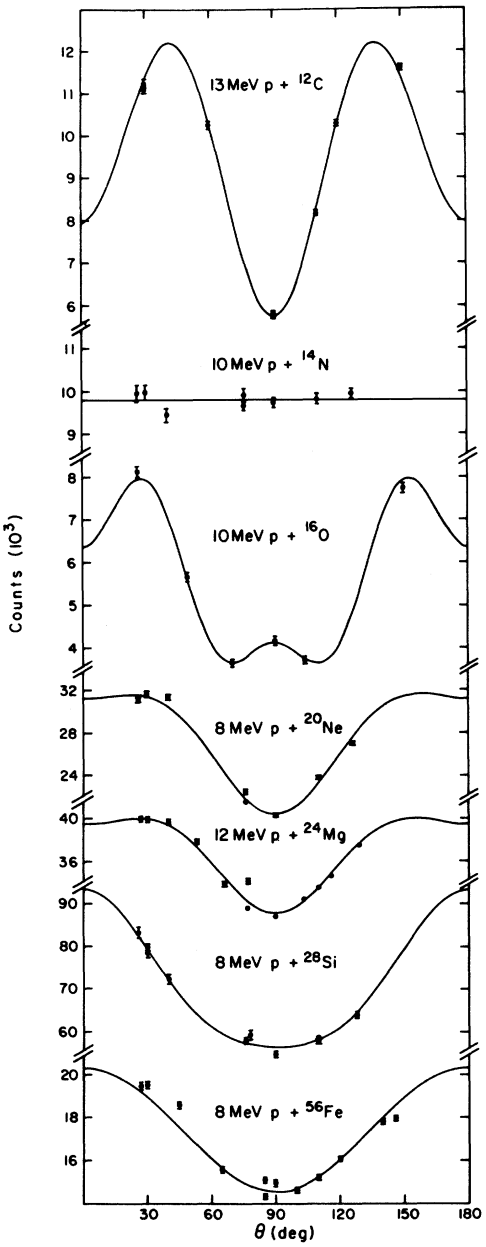

FIG. 2. Examples of angular distributions of gamma rays. The solid curves are fits with an expansion in Legendre polynomials of even order through zero for the ^{14}N case, through 6 for the ^{16}O case, and through 4 for the other cases. The gamma-ray energies (top to bottom) are 4.44, 2.31, 6.13, 1.63, 1.37, 1.78, and 0.847 MeV.

In order to correct for possible target thickness errors, two "normalization" series of runs were taken, one with the 1.8 mg/cm^2 target and one with a thinner target of uniform thickness. The normalization runs differed from the "excitation function" runs in that in the former a broad span of energies was covered in relatively large steps. Comparisons of the excitation function runs to the normalization runs suggested that there had been an (unexplained) shift in system performance above about 15 MeV, corresponding, for example, to deduced cross sections which were 7% too high above 15 MeV or 7% too low below 15 MeV.

To explore this anomaly further and to obtain an independent absolute cross section determination, the total inelastic cross section to the 4.44-MeV level was determined at 12 MeV by measuring the angular distribution of scattered protons from 10° to 170° in 10° steps. One movable and three fixed monitor Si(Li) detectors were used in this measurement. A specially prepared carbon target of uniform thickness was used for this run; its thickness was determined to be 1.93 mg/cm^2 by using an α-source thickness gauge. A check of the thickness determination was performed during the experiment by using three carbon targets of different measured thicknesses; the yields of scattered protons were observed to scale with the measured thicknesses. As a check on our detector geometry and beam integration, we measured the Rutherford scattering cross section for 6-MeV protons on a Au target. At all angles studied, our measured cross sections deviate from the Rutherford cross sections by less than 2%. The total inelastic cross section to the ^{12}C 4.44-MeV level was determined by integrating the measured angular distribution. The cross section was found to be 267 ±14 mb, in good agreement with the cross section for gamma-ray production, which had previously been found to be 262 mb in the excitation function run at 12 MeV.

Based on this measurement and on comparisons at other energies between the excitation function runs and the normalization runs, the 4.44-MeV cross sections were renormalized, increasing the previously determined cross sections by 2% below 15.2 MeV, and decreasing them by 5% above 15.2 MeV.

III. CONTRIBUTIONS FROM (p,n) AND (p,$2n$) REACTIONS

A. General

It has been tacitly assumed that the gamma rays of interest are produced in inelastic proton scattering reactions, either to the parent state or after a gamma-ray cascade to the parent state. However, the same gamma-ray lines can in most cases be produced by (p,n) reactions, followed by positron emission or electron capture. [Aside from the 0.812-MeV line from ^{56}Co, produced in the ^{56}Fe(p,n)^{56}Co reaction, lines from (p,n) reactions themselves are not very strongly excited, and are not considered in the present work.]

With the exception of the $^{14}N(p,n)\,^{14}O$ and $^{56}Fe(p,n)\,^{56}Co$ cases, the ground states of nuclei produced in the (p,n) reactions have half-lives too short (2 sec or less) for a distinction between the (p,p') and (p,n) channels to be relevant, because both in the astrophysical environments and in the laboratory cross section measurements, the gamma rays from the (p,p') and (p,n) reactions are emitted in times that are short compared to other time scales. Therefore, no attempt is made to separate the (p,p') and (p,n) contributions except for the ^{14}O and ^{56}Co cases. These are discussed in Secs. III B and III C below. The $^{56}Fe(p,2n)\,^{55}Co$ reaction is considered in Sec. III D.

B. Measurement of the $^{14}N(p,n)^{14}O(\beta^+)^{14}N$ reaction cross section

The half-life of ^{14}O is 70.6 sec, and the ^{14}O branching ratio to the 2.31-MeV state of ^{14}N is 99.3%.[13] Therefore, it can be anticipated that there will be a significant ^{14}O contribution to the 2.31-MeV gamma-ray yield for protons above the reaction threshold at 6.355 MeV (lab). Typical counting times in the proton bombardments of ^{14}N were in the neighborhood of 10 min, with an interval of several minutes between successive runs. Most, but not all, of the ^{14}O contribution was therefore included in the routine counting of the 2.31-MeV gamma rays.

To permit an estimate of the number of ^{14}O events, a measurement was made of the cross section for producing 2.31-MeV gamma rays from the $^{14}N(p,n)\,^{14}O(\beta^+)\,^{14}N$ reaction. A Ge(Li) detector was used (at 110°, 21 cm from the target) in the same experimental configuration as was used for the $^{14}N(p,p')\,^{14}N$ measurements.

The thickness of the nitrogen in the gas cell was 2.5 mg/cm^2 and the exit foil was 1.8 mg/cm^2 thick, so that recoiling ^{14}O nuclei were stopped either in the gas or in the cell wall or exit foil. To verify that the effective half-life of the ^{14}O decay equaled the known decay rate, the target was bombarded with a 10-MeV beam, and gamma rays were counted for 20 sec intervals, at times beginning 5, 40, 80, and 120 sec after termination of the bombardment. The relative number of counts in the four intervals agreed with that expected from ^{14}O decay, within the statistical errors (about 10%). (The effective half-life was not expected to be significantly different from the ^{14}O half-life, because the pressure in the gas cell was maintained through a side tube, not by direct flow through the cell.)

The procedure for measuring the (p,n) cross section, as well as simultaneously measuring the (p,p') cross section, was as follows: The beam was turned on for a period of more than 8 min, after which gamma rays were counted for 300 sec and the beam current was integrated; after the beam had been turned off for 5 sec, gamma rays were counted for another 300 sec. A pulser was used to correct for dead time. Cross sections for the production of 2.31-MeV gamma rays from the (p,n) and (p,p') reactions were thus determined. [Since the 2.31-MeV state has spin 0, gamma rays from the (p,p') reaction, as well as the delayed gamma rays, were isotropic.] These measurements were made at proton energies from 7 to 22 MeV at 1- or 2-MeV intervals.

The measured cross section for the $^{14}N(p,n)\,^{14}O(\beta^+)\,^{14}N$ reaction is plotted in Fig. 3. The uncertainty in absolute cross section determination is about 10%. At all energies below 22 MeV, the cross section for the production of 2.31-MeV gamma rays from the (p,n) reaction is less than 15% of the cross section for production via the (p,p') reaction (see Sec. IV), and over most of the range it is under 10%. Furthermore, the counting times were usually in the neighborhood of 10 half-lives of ^{14}O, and there was some contribution to the measured counts from ^{14}O formed before the counting interval was started, making the effective loss of (p,n) gamma rays less than 10%. In consequence, the correction for lost (p,n) events was small. A more detailed analysis shows that in no case was it as much as 2% of the total number of 2.31-MeV gamma rays [from the (p,p') and (p,n) reactions combined] and in most cases it was under 1%. A correction was inserted on an overall basis, rather than on a run-by-run

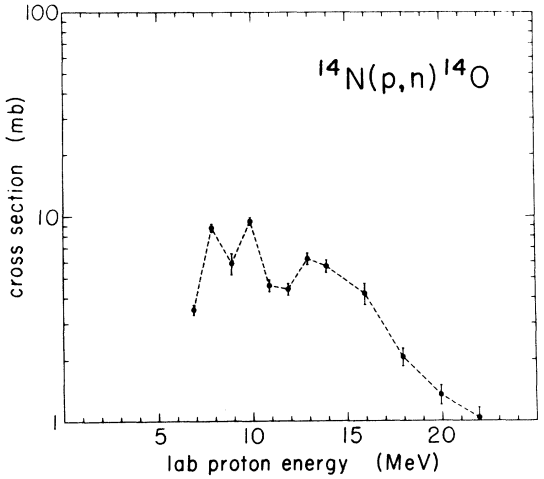

FIG. 3. Cross section for the $^{14}N(p,n)^{14}O$ reaction, obtained by measuring yields of delayed 2.31-MeV gamma rays. (The lines connecting the data points in this and succeeding figures are intended only to guide the eye.)

basis, by multiplying all measured yields by a correction factor of 1.01 ± 0.01. This gives the summed cross section for the production of 2.31-MeV gamma rays by (p,p') and (p,n) events.

The $^{14}N(p,n)\,^{14}O$ cross sections determined in this experiment are much lower than the cross sections reported by Kuan and Risser,[14] who made a similar measurement from threshold to 12 MeV. The discrepancy is largest at the higher end of the range of energies covered in the earlier work. At 12.0 MeV, Kuan and Risser report a cross section greater than 100 mb, while in the present work the measured cross section is 4.4 mb.

These results can also be compared to unpublished measurements for the $^{14}N(p,n)\,^{14}O_{g.s.}$ reaction at 12.2 MeV quoted by Richter and Parish.[15] They plot measured differential cross sections for neutrons to the ground state of ^{14}O. The integrated cross section is roughly 4.2 mb, in good agreement with the present result. It is very unlikely that there is any appreciable contribution to the ^{14}O production cross section at 12.0 MeV from (p,n) reactions to excited states. The threshold for the (p,n) reaction to the 5.17-MeV first excited state of ^{14}O is at $E_p = 11.89$ MeV, and this state is unstable to proton emission (its decay modes have apparently not been determined experimentally). The currently measured cross sections for the (p,n) reaction are flat from 11 to 16 MeV, lying between about 4 and 6 mb, and there is no sign of any increase at 12.0 MeV which could be attributed to the opening of the excited state channel.

A comparison can also be made between the $^{14}N(p,n)\,^{14}O_{g.s.}$ and $^{14}N(p,p')\,^{14}N_{2.31\text{-MeV}}$ cross sections. The 2.31-MeV state of ^{14}N is the isotopic analog of the ^{14}O ground state. The two cross sections are related through isospin symmetry, by which, apart from kinematic and Coulomb corrections, the ratio of the (p,n) to (p,p') cross sections should be 2. The (p,p') cross sections have been measured by Shrivastava *et al.* [16] from 6 to 9 MeV and by Hansen *et al.* [17] from 8.5 to 14.6 MeV. The (p,p') results are in rough agreement with our (p,n) results. For example, in the interval between 11 and 14.6 MeV, where the corrections are expected to be smallest, the (p,p') cross sections average about 3.5 mb, while the (p,n) cross sections average about 5 mb.

C. Measurement of the $^{56}Fe(p,n)^{56}Co$ reaction cross section

The cross section for the $^{56}Fe(p,n)\,^{56}Co$ reaction was measured by bombarding stacks of iron foils with protons and counting delayed gamma rays from the decay of ^{56}Co, which has a half-life of 78.8 d.[18] The reaction threshold is 5.446 MeV (lab).

The bombardment was carried out in a 1.52-m diameter scattering chamber. A Si(Li) particle detector was mounted at 45° to the beam, and a gold foil was mounted on a target ladder in the center of the chamber. Also mounted on the target ladder, but 7 cm off center, was a stack of iron foils. The target ladder could be rotated so that the iron foils could be placed upstream or downstream of the gold foil, or could be rotated out of the beam path. Apertures were placed in front of the particle detector, so that only particles scattered from the gold foil (not from the iron foils) were detected.

The iron foils were of natural composition, with a purity of 99.5%. Thicknesses were 20.5 mg/cm^2, measured by weighing selected foils. Stacks of 8, 12, 15, and 18 foils were bombarded by beams of energies 10.0, 14.5, 19.2, and 23.0 MeV, respectively; the beam energies after passing through the stacks were 3.8, 8.1, 12.9, and 16.4 MeV, respectively. This allowed us to measure the $^{56}Fe(p,n)\,^{56}Co$ cross section from threshold to 22.8 MeV, in steps of 1.0 to 0.3 MeV, with overlap of a few measurements made with different stacks.

The bombardment procedure was designed so that we could infer the integrated beam current without requiring charge integration of the beam while it passed through the iron stack, and so that we could measure the beam energy loss in the stack. With the iron stack rotated out of the path of the beam, we first measured the number of protons scattered by the gold foil, while integrating the beam in the Faraday cup of the chamber. This calibrated the beam flux against scattered protons. We next rotated the iron foil stack into a position upstream from the gold foil, and, with a very short bombardment, measured the energy of the particles scattered into the detector by the gold foil after the beam had passed through the iron stack (to determine the beam energy loss in the stack). The stack was then placed downstream of the gold foil, and the iron foils were bombarded for about 2 h with about 100 nA of beam current. During this time, particles scattered from the gold foil were counted by the Si(Li) detector. At the end of the bombardment, the charge calibration was repeated. Finally, the incident beam energy was lowered to that of the iron-stack exit energy, and the position of the peak of particles scattered from the gold foil was recorded for calibration of the particle detector spectrum.

The amount of ^{56}Co activity produced in the foils was measured by counting gamma rays from

the foils 18 d after the bombardment and (from several foils at about 2 MeV proton energy intervals) 49 d after the bombardment. Foils were counted with a Ge(Li) detector, the efficiency of which was calibrated using ^{56}Co and other standard sources.

For each spectrum, we extracted yields for 0.847- and 1.238-MeV gamma rays. Ratios of these gamma yields were constant to within 5%. Count rates measured 49 d after the bombardment were consistent with those measured after 18 d to within 5%, assuming a 78.8 d half-life.

Cross sections determined from the four foil stacks overlapped in three energy regions. Discrepancies of up to 5% could not be accounted for, and the data from the different stacks were arbitrarily renormalized by increasing cross sections below 9 MeV by 2.5% and decreasing those above 9 MeV by about 2.5%.

Energies at which cross sections are quoted are bombarding energies at the center of the foil. These energies were determined by measurements of the energies of protons scattered by the gold foil, with and without the iron stack upstream of the gold foil. The values were at most 160 keV different from energies calculated from energy loss tables and the foil thicknesses obtained by weighing the foils (the largest differences being those of the exit foils in each stack).

The resulting ^{56}Fe(p,n) ^{56}Co excitation function is shown in Fig. 4. Cross section uncertainties are about 5% for relative errors and about 10% for absolute values.

Our ^{56}Fe(p,n) ^{56}Co cross sections are about 10% lower than those of Tanaka and Furukawa,[19] and about 20% higher than those of the more recent measurement by Jenkins and Wain.[20] A comparison of our results to those of Williams and Fulmer[21] reveals a difference in shape of the excitation function: Our cross sections are considerably higher than those of Williams and Fulmer at energies below 16 MeV and somewhat lower at higher energies. Cross sections at two energies in this range have been measured by Brodzinski *et al.*[22]; their cross section agrees with ours at 14.1 MeV, but is 30% lower at 15 MeV.

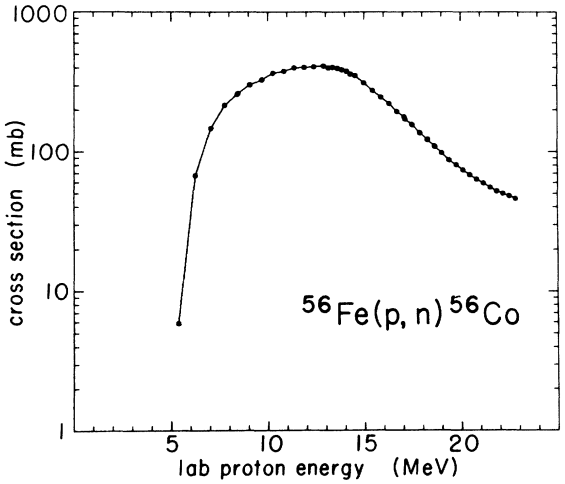

FIG. 4. Cross section for the ^{56}Fe(p,n)^{56}Co reaction, obtained by measuring yields of delayed 0.85-MeV gamma rays.

The ^{56}Co decay results in emission of a 0.847-MeV gamma ray more than 99.9% of the time, a 1.238-MeV gamma ray 67% of the time, and a 1.811-MeV gamma ray 0.65% of the time.[18] Because of the long ^{56}Co half-life, the 0.847- and 1.238-MeV gamma-ray yields are tabulated below, both for the prompt (p,p') gamma ray cross section alone and with the ^{56}Co decay contribution added. Activity from ^{56}Co built up in the target was determined not to have contributed significantly to the measured prompt gamma-ray yield.

D. Corrections for the ^{56}Fe(p,$2n$)^{55}Co reaction

The measured yields for the 0.931-MeV and the 1.317-MeV lines from the ^{56}Fe(p,pn) ^{55}Fe reaction include some contribution from decay of ^{55}Co($t_{1/2}$ = 17.5 h) which is produced in the ^{56}Fe(p,$2n$) ^{55}Co reaction. The magnitude of this cross section has been measured by Jenkins and Wain.[20] Using these cross sections and the time history of the bombardment of the ^{56}Fe target, it was possible to deduce the contribution of ^{55}Co buildup to the observed yields. The contribution increased with time during the run, amounting for the 0.931-MeV line to the equivalent of a 1 mb correction at the beginning of the run and a 5 mb correction at the end. These corrections were subtracted from the observed 0.931-MeV "cross sections"; the correction was trivial at the higher energies where the (p,pn) contribution exceeded 200 mb, but amounted to about one-third of the yield at 14.9 MeV, the lowest energy at which the cross section was extracted. The 1.317-MeV line has a strength less than one-tenth that of the 0.931-MeV line in the decay of ^{55}Co, and thus only a very small correction was required in this case.

The final results plotted in Fig. 13 below are the cross sections for the (p,pn) reaction only. This suffices for the 1.317-MeV line under any reasonable circumstances. However, the (p,$2n$) contribution can be significant for the 0.931-MeV line. Average cross sections are presented in Table II for both the (p,pn) reaction alone and for the sum of the (p,pn) and (p,$2n$) reactions, using the data of Jenkins and Wain[20] for the latter.

TABLE II. Cross sections (in mb) for the production of gamma rays in proton-induced reactions. The cross sections are averaged over 1-MeV-wide bins centered at the indicated proton energies.

Target nucleus	^{12}C	^{16}O	^{14}N	^{14}N	^{16}O	^{20}Ne	^{20}Ne	^{24}Mg	^{24}Mg	^{28}Si	^{56}Fe	^{56}Fe	^{56}Fe	^{56}Fe	^{56}Fe	^{56}Fe	^{56}Fe	^{56}Fe	^{56}Fe
Residual nucleus	^{12}C	^{12}C	^{14}N	^{14}N	^{16}O	^{16}O	^{20}Ne	^{20}Ne	^{24}Mg	^{28}Si	^{55}Fe	^{55}Fe	^{55}Fe	^{56}Fe	^{56}Fe	^{56}Fe	^{56}Fe	^{56}Fe	^{56}Co
E_γ (MeV)	4.44	4.44	1.63	2.31	6.13	6.13	1.63	1.63	1.37	1.78	0.931	0.931	1.317	0.847	0.847	1.238	1.238	1.811	0.812
Beta decay included?[a]	Yes	NA[a]	Yes	Yes	NA	NA	Yes	NA	Yes	Yes	No	Yes	No	No	Yes	No	Yes	No	NA
E_p=2 MeV																			
3							158		25										
4				9			133		107	73									
5			5	15			265		322	140				135	135			6	
6	55		30	36			422		377	217				253	298	19	49	28	
7	108		65	84			555		442	292				294	439	36	133	36	46
8	240		54	93	38		367		456	307				335	568	66	222	44	82
9	290		50	80	69		337		490	352				357	656	91	291	44	98
10	265		67	106	97		319		550	379				385	737	114	350	51	114
11	317		55	95	122		330		497	408				405	785	134	389	51	116
12	270		41	71	160		326		540	421				444	849	161	432	51	112
13	282		31	61	163		318		501	410				456	861	180	451	51	102
14	281	3	26	53	130		296		500	384				462	844	194	450	48	78
15	217	16	24	43	128		246		476	391	16	16		449	762	202	412	43	57
16	193	40	19	36	115		225		429	352	56	61	29	423	661	197	356	39	42
17	169	64	15	33	107	71	215	31	363	312	103	116	57	380	558	183	302	35	31
18	156	85	13	30	97	93	202	68	317	284	145	165	89	324	456	155	243	30	23
19	140	123	13	28	92	108	177	105	281	245	179	206	124	278	377	128	194	28	19
20	125	140	12	24	82	103	157	136	255	207	206	240	155	243	319	107	158	24	14
21	118	150		22	72	104	141	161	241	180	223	259	179	215	277	89	131	22	14
22	110	156		21	59	101	129	171	215	164	234	274	194	201	252	77	111	23	12
23	107	157		21	58	90	128	180	208	151	236	280	202	186	230	68	97	22	11

[a] Inclusion of beta decay gives contribution from (p,n) or $(p,2n)$ reactions.
[b] Not applicable.

IV. RESULTS

A. Present measurements

At the lowest proton bombarding energies, the gamma-ray spectra are fairly simple, with one or two strong lines; however, with increasing bombarding energy, more reaction thresholds are reached and more excited states in the residual nuclei can be populated, so that a greater number of gamma rays are observed in the spectra. The primary criterion used in selecting which of these gamma rays to analyze was large cross section. Usually, the strongest gamma-ray lines came from the first-excited-state to ground-state transitions in the target nucleus, following the (p,p') reaction; sometimes second- to first-excited-state transitions were also strong. In ^{16}O, the 0^+ first excited state at 6.05 MeV decays by electron pair emission, and the strongest gamma-ray line comes from the ground-state transition of the 6.13-MeV 3^- second excited state.

For the ^{16}O, ^{20}Ne, and ^{24}Mg targets, we also extracted cross sections for the $(p,p\alpha)$ reactions producing the same gamma rays as the (p,p') reactions on the ^{12}C, ^{16}O, and ^{20}Ne targets, respectively. These two yields must be added in comparing to astronomical observations. [Cross sections for the $(p,p\alpha)$ reaction on ^{28}Si were not obtained because there was a significant background of (p,α) events arising from stray beam striking aluminum in the scattering chamber.] Cross sections for several lines from $p+^{56}Fe$ were extracted, including that for 0.812-MeV gamma rays produced by the $^{56}Fe(p,n)\,^{56}Co$ reaction, a line not copiously produced by alpha-particle-induced

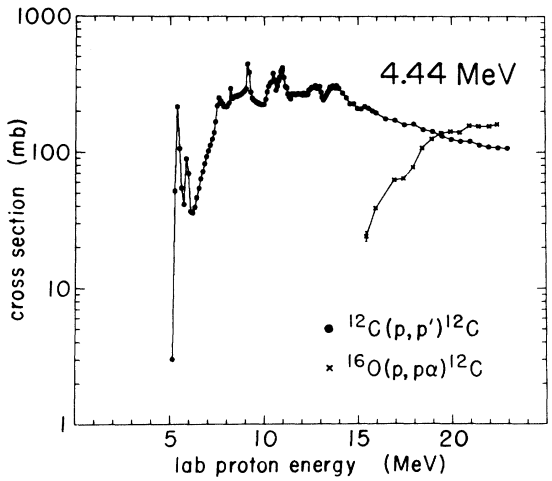

FIG. 5. Cross sections for production of 4.44-MeV gamma rays from $p+^{12}C$ and $p+^{16}O$ reactions. [Note: In Figs. 5–10, the delayed contribution from (p,n) reactions followed by β^+ decay is included, when present.]

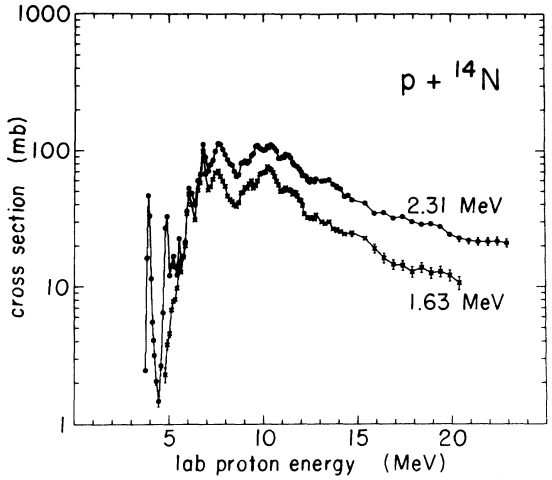

FIG. 6. Cross sections for production of 2.31- and 1.63-MeV gamma rays from $p+^{14}N$ reactions.

reactions. Two cross sections for delayed activity were also measured: $^{14}N(p,n)\,^{14}O$ and $^{56}Fe(p,n)\,^{56}Co$ (see Sec. III).

The excitation functions for gamma-ray production are presented in Figs. 5 through 13. Data points are plotted at (lab) proton energies corresponding to the target center. The solid lines in the plots merely connect the data points.

The excitation functions for the lighter targets, shown in Figs. 5 through 10, correspond to the sum of the yields from the (p,p') and (p,n) reactions, except for ^{16}O (where ^{16}F is particle unstable). Excitation functions for ^{56}Fe are shown in Figs. 11 through 13. The cross sections in Fig. 11 are for the (p,p') reactions alone, for lines at 0.847, 1.238, and 1.811 MeV. The total yields for the 0.847- and 1.238-MeV lines, including the contribution from the $^{56}Fe(p,n)\,^{56}Co(\beta^+EC)\,^{56}Fe$

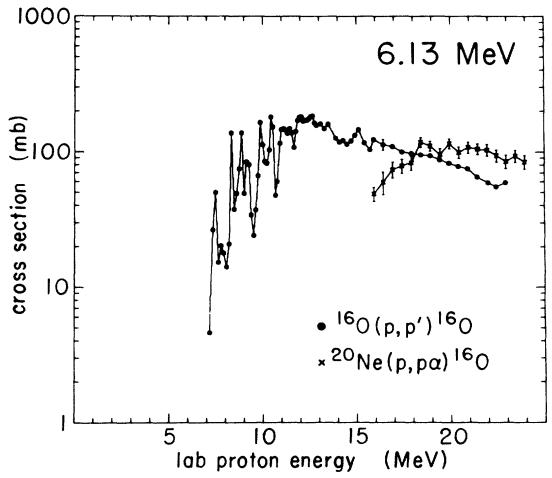

FIG. 7. Cross sections for production of 6.13-MeV gamma rays from $p+^{16}O$ and $p+^{20}Ne$ reactions.

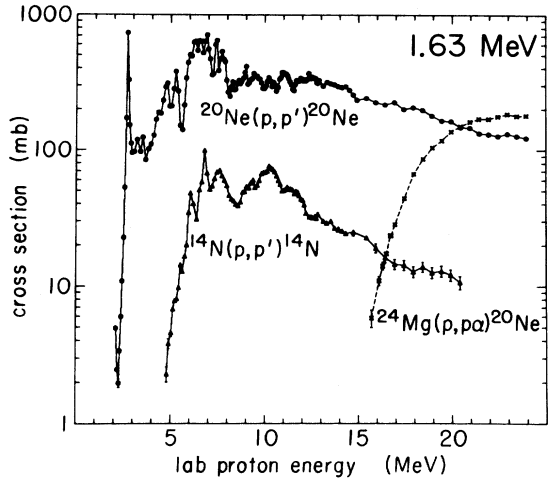

FIG. 8. Cross sections for production of 1.63-MeV gamma rays from $p + {}^{20}$Ne, $p + {}^{24}$Mg, and $p + {}^{14}$N reactions. Gamma rays from the ^{24}Mg$(p, 2p)^{23}$Na reaction are included with the ^{24}Mg$(p, p\alpha)^{20}$Ne gamma rays.

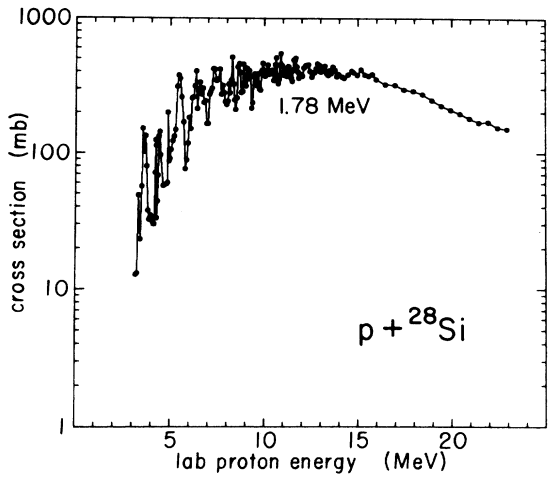

FIG. 10. Cross sections for production of 1.78-MeV gamma rays from $p + {}^{28}$Si reactions.

reaction, are compared in Fig. 12 to the (p,p') yield (the branching ratio for the 1.811-MeV line in ^{56}Co decay is less than 1%). The excitation functions for the prompt 0.812-MeV line from the ^{56}Fe(p,n) ^{56}Co reaction and for the 0.931- and 1.317-MeV lines from the ^{56}Fe(p,pn) ^{55}Fe reaction are shown in Fig. 13. The delayed contributions from the ^{56}Fe$(p,2n)$ ^{55}Co$(\beta^+\text{EC})$ ^{55}Fe reaction are not included in Fig. 13; this contribution is small for the 0.931-MeV line (see Table II) and negligible for the 1.317-MeV line.

Error bars shown in these figures are for statistical errors only. Errors in the determination of absolute cross sections arise from errors in yield extraction (generally 5%, but larger at the higher proton energies), beam current integration (estimated at 3%), target thickness measurement (ranging from 5% to 13%; see Table I), and Ge(Li) efficiency measurement (estimated at 5% for low-energy gamma rays and 10% for the 4.44- and 6.13-MeV gamma rays). These errors are added quadratically to give the approximate absolute errors quoted in Table III. The error quoted for the $p + {}^{12}$C reaction, yielding 4.44-MeV gamma rays, is slightly smaller than that given by the quadratic sum, because of the special normalization procedure described in Sec. II F.

In many cases a gamma ray can be produced by more than one reaction. An example is the 4.44-MeV gamma ray, which can be produced by the

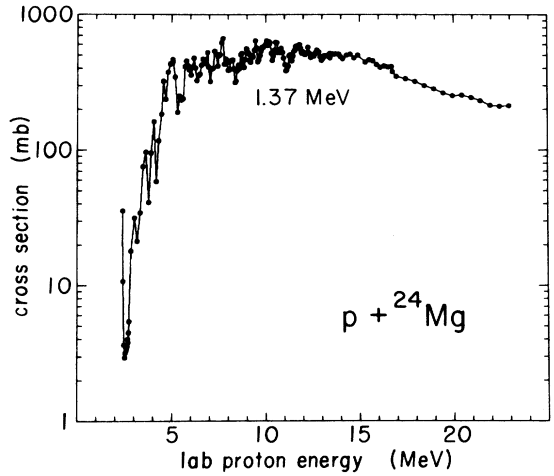

FIG. 9. Cross sections for production of 1.37-MeV gamma rays from $p + {}^{24}$Mg reactions.

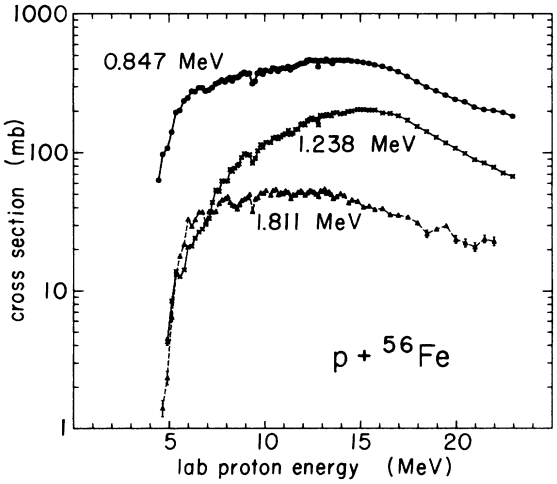

FIG. 11. Cross sections for production of 0.847-, 1.238-, and 1.811-MeV gamma rays from the ^{56}Fe(p,p') ^{56}Fe reaction.

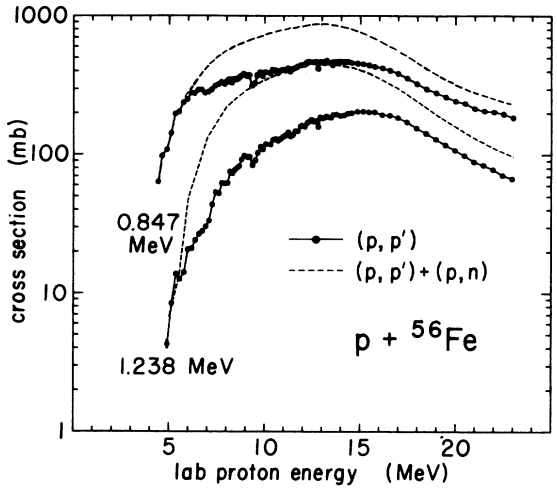

FIG. 12. Comparison of cross sections for production of gamma rays from ^{56}Fe. The solid curves correspond to the ^{56}Fe$(p,p')^{56}$Fe reaction alone; the dotted curves correspond to the sum of the ^{56}Fe$(p,p')^{56}$Fe and ^{56}Fe $(p,n)^{56}$Co$(\beta^+ \mathrm{EC})^{56}$Fe yields.

^{12}C(p,p') ^{12}C and ^{16}O$(p,p\alpha)$ ^{12}C reactions. We have plotted all measured cross sections for a given gamma ray in one figure. A gamma ray near 1.635 MeV can be produced from the decay of the first excited state of ^{20}Ne (E_γ = 1.634 MeV), from the decay of the second excited state of ^{23}Na to the first excited state (E_γ = 1.636 MeV), and from the decay of the second excited state of ^{14}N to the first excited state (E_γ = 1.635 MeV). There are thus four major sources for this gamma ray from proton-induced reactions: ^{20}Ne(p,p') ^{20}Ne,

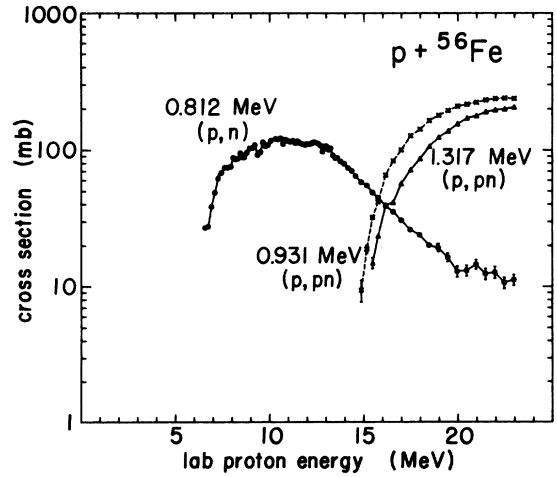

FIG. 13. Cross sections for the production of 0.812-MeV gamma rays from the ^{56}Fe$(p,n)^{56}$Co reaction and of 0.931- and 1.317-MeV gamma rays from the ^{56}Fe $(p,pn)^{55}$Fe reaction.

TABLE III. Estimated uncertainties in the determination of absolute gamma-ray production cross sections in proton-induced reactions.

Target	E_γ (MeV)	Uncertainty
^{12}C	4.44	10%
^{14}N	2.31	10%
^{14}N	1.63	10%
^{16}O	6.13	15%
^{16}O	4.44	15%
^{20}Ne	1.63	10%
^{20}Ne	6.13	25%
^{24}Mg, <2.8 MeV	1.37	15%
^{24}Mg, >2.8 MeV	1.37	10%
^{24}Mg	1.63	10%
^{28}Si, <5 MeV	1.78	15%
^{28}Si, >5 MeV	1.78	10%
^{56}Fe	all	15%

^{24}Mg$(p,p\alpha)$ ^{20}Ne, ^{24}Mg$(p,2p)$ ^{23}Na, and ^{14}N(p,p') ^{14}N.

In the case of data acquired with natural targets (carbon, nitrogen, oxygen, neon, and silicon), yields of gamma rays produced by (p,d) and (p,t) reactions on the heavier isotopes are included in the cross sections. For astrophysical sources in which the isotopic abundances are the same as those on earth, these are the cross sections required. The difference, however, is small (less than about 1%), as the (p,d) and (p,t) reaction cross sections are expected to be at least several times smaller than those of the (p,p') reaction, and the isotopic abundances of the heavier isotopes are small.

In order to have the data in a form convenient for comparison with astrophysical observations, we have averaged the cross sections over 1-MeV-wide energy bins. The results are given in Table II. In addition to the cross sections presented in the main tables and graphs, we have investigated several specific questions relating to other cross sections of interest, including $(p,p\alpha)$ yields for ^{28}Si and ^{56}Fe targets.

(a) The ^{16}O(p,pn) ^{15}O and ^{16}O$(p,2p)$ ^{15}N reactions to states at 5.183 and 5.241 MeV in ^{15}O and at 5.270 and 5.299 MeV in ^{15}N are reported to (together) have sizable gamma-ray yields at higher energies.[1,23] There were no signs of these lines in the present work. At 23 MeV, an upper limit of 15 mb can be put on the possible ^{15}N contribution. The threshold for reaching the lowest ^{15}O state is at E_p = 22.1 MeV, and therefore the yield from the ^{15}O lines can be assumed to be negligible at E_p = 23 MeV.

(b) Although the determination of the excitation function for the 1.37-MeV line from the ^{28}Si$(p,p\alpha)^{24}$Mg reaction was made difficult by the

presence of a background contamination from the $^{27}Al(p,\alpha)^{24}Mg$ reaction, it was possible to make an approximate determination of this cross section at the higher energies studied. At 23 MeV, the cross section is roughly 90 ± 25 mb, which is smaller than the cross sections for the $(p,p\alpha)$ reaction on ^{16}O and ^{24}Mg, and about the same as that for ^{20}Ne.

(c) The cross section for the production of 1.434-MeV gamma rays from the $^{56}Fe(p,p\alpha)^{52}Cr$ reaction is reportedly very appreciable at 100 MeV.[1,24] We have looked for this line at the lower energies of the present measurement. It was necessary to distinguish between the 1.434-MeV ^{52}Cr line and a 1.441-MeV line arising from the $^{56}Fe(p,\alpha)^{53}Mn$ reaction; this was done by fitting two Gaussian pulse shape distributions to the poorly resolved double peak. The cross sections for both lines are quite low below 14 MeV. They rise steeply between 14 and 20 MeV, with the cross section for the 1.441-MeV line being the larger until near 20 MeV. At 20 MeV, the two cross sections are each about 10 mb. Above 20 MeV, the 1.434-MeV excitation function continues to rise, with the cross section reaching (44 ± 10) mb at 23 MeV, while the excitation function for the 1.441-MeV line is essentially flat between 20 and 23 MeV.

B. Comparison to other measurements

A few gamma-ray production cross sections in this energy range have been measured previously by Zobel *et al.*,[23] using NaI(TI) detectors. Most yields were measured at $\theta_\gamma = 135°$, and the angular distributions required for extraction of total cross sections are not available. In the case of 14.6-MeV $p + {}^{12}C$, yielding 4.44-MeV gamma rays, measurements were made at three angles; however, the results are not self-consistent. The differential cross section at 135° was found to be 8 times greater than that at 50°, although these cross sections should be about equal, since the angular distribution must be symmetric about 90°. A comparison of Zobel's ^{12}C differential cross sections to our results shows the Zobel result to be 2 times larger at 135°, about the same at 90°, and 3.5 times smaller at 50°. For 12.1-MeV $p + {}^{16}O$, yielding 6.13-MeV gamma rays, the thick target and the lack of angular distribution information in the Zobel measurement makes comparison difficult, but agreement seems to be good to 20%. The Zobel results for 15.7-MeV $p + {}^{56}Fe$, yielding 0.85- and 1.24-MeV gamma rays, are somewhat higher than our results, but within the errors of the Zobel measurement (assuming an isotropic angular distribution; the distribution has not been measured).

Aside from the survey by Zobel *et al.*, there are few reported results on total cross sections for gamma-ray yields. In one further comparison, we find that our cross sections for production of 2.31-MeV gamma rays from the $p + {}^{14}N$ reaction are in general agreement (maximum differences about 30%) with those of Phillips *et al.*,[25] who measured yields of 2.31- MeV gamma rays with a Ge(Li) detector, up to proton energies of 6.4 MeV (lab).

For the 4.44-MeV line of ^{12}C and, to a lesser extent, the 6.13-MeV line of ^{16}O, it is possible to compare the gamma-ray cross sections with measured inelastic proton scattering cross sections. For ^{12}C, the higher excited states decay primarily by breakup into alpha particles; at proton energies below 23 MeV their excitation contributes less than 0.5 mb to the 4.44-MeV gamma ray yield.[26] Therefore, the inelastic scattering cross section and the gamma-ray cross section are almost equal. The present results give gamma-ray cross sections which are somewhat higher than previously measured (p,p') cross sections. At low energies, comparisons are made somewhat uncertain by differences in bombarding energies and target thicknesses. We estimate that our cross sections are about 10% above the (p,p') cross sections reported by Barnard, Swint, and Clegg[27] between 6 and 10 MeV, and about 4% above the (p,p') cross sections of Swint *et al.*[28] near 9.2 MeV. At 12 MeV, our measured (p,p') cross section of 267 ± 14 mb lies 8.5% above the value of 246 ± 6 mb reported by Conzett.[29] The present gamma-ray cross sections are on the average about 8% above the (p,p') cross sections at 15 to 19 MeV of Daehnick and Sherr,[12] and about 2% above the (p,p') cross sections of Dickens[30] near 20 MeV. [Our results include a correction, always under 3%, for 4.44-MeV gamma rays from the $^{16}O(p,p\alpha)^{12}C$ reaction on an oxygen contaminant in the carbon target. No correction has been made for gamma rays from the $^{13}C(p,pn)^{12}C$ reaction, because it is believed to be highly unlikely that the fractional gamma-ray contribution from ^{13}C exceeds the 1% relative abundance of ^{13}C in the (natural) carbon target.]

At proton energies below 9.4 MeV (the threshold for producing the 8.87-MeV state of ^{16}O), the cross sections for the production of 6.13-MeV gamma rays are essentially the same as those for inelastic scattering to the 6.13-MeV state of ^{16}O. Our cross section at 9.2 MeV agrees with the (p,p') cross section of Dangle *et al.*,[31] lying about (4 ± 10)% above the cross section inferred from their plot of the Legendre polynomial coefficient a_0 for scattering to the 6.13-MeV state.

Ramaty *et al.*[1] have recently compiled an exten-

sive set of cross sections relevant to gamma-ray astronomy. These cross sections were derived primarily from cross sections for inelastic proton scattering and gamma-ray branching ratios, with some input from gamma-ray measurements. The Ramaty results and the results of the present work cannot be considered independent determinations of the cross sections, however, because our preliminary data were available to Ramaty *et al.*, and some of their cross section determinations were influenced by the present measurements. The cross sections quoted by Ramaty *et al.* are typically within 20% of our results, with occasional 50% differences, for gamma rays from inelastic proton scattering on ^{12}C, ^{16}O, ^{20}Ne, ^{24}Mg, ^{28}Si, and ^{56}Fe nuclei, and for gamma rays from the $(p,p\alpha)$ reactions on ^{16}O, ^{20}Ne, and ^{24}Mg targets [in the ^{24}Mg case, including any $(p,2p)$ gamma rays of energy 1.64 MeV]. The cross sections for producing 2.31-MeV gamma rays from the $p+^{14}$N reaction, as given by Ramaty, are about twice our cross sections for lab proton energies between 8 and 15 MeV, because Ramaty *et al.* used the rather large cross sections for the ^{14}N$(p,n)^{14}$O reaction given by Kuan and Risser[14] (see Sec. III B). Our cross section for producing 1.37-MeV gamma rays from the ^{28}Si$(p,p\alpha)^{24}$Mg reaction at 23 MeV is three times smaller than that of the Ramaty estimate. For the case of 1.434-MeV gamma rays produced by the ^{56}Fe$(p,p\alpha)^{52}$Cr reaction at 23 MeV, our cross section is about 8 times smaller than the Ramaty estimate.

C. Cross sections averaged over proton spectra

The prominence of individual gamma-ray lines from astrophysical sources will depend upon the target abundances, the energy spectra of the protons, and the cross sections as a function of energy. To aid in predicting the relative importance of the different gamma-ray lines, we have followed a common practice in the treatment of low energy particle spectra, and have averaged the cross sections over a power law spectrum in proton kinetic energy, of the form

$$\phi(E)\propto E^{-s}, \quad E\geq E_c$$
$$\phi(E)=0, \quad E<E_c. \tag{2}$$

The average cross section is defined as

$$\langle\sigma\rangle=\frac{\int_{E_c}^{\infty}\sigma(E)E^{-s}dE}{\int_{E_c}^{\infty}E^{-s}dE}. \tag{3}$$

The power law exponent s is considered to be a variable parameter. The cutoff energy E_c serves as an artifact to avoid infinite flux at zero energy. We set $E_c=2$ MeV. Because the cross sections for all reactions considered here are negligible (usually zero) below 2 MeV, this implies integration over the full power law spectrum upward from the reaction threshold. The choice of E_c thus affects only the denominator in Eq. (3); it provides an arbitrary overall normalization which applies equally to all reactions.

Cross sections, averaged in this manner over power law spectra, are presented in Table IV for several values of the parameter s. In calculating these average cross sections, it was necessary to estimate cross sections for proton energies above 23 MeV (the usual upper limit of our measurement). When possible, these extrapolated cross sections were based on measurements in the literature. For the (p,p') and (p,n) reactions, most of the yield arises from interactions below 23 MeV (for $s\gtrsim 2$), and the uncertainty in the extrapolated cross sections introduces negligible error. For other reactions, the results are less certain. This point is brought out more quantitatively in Table V, where we present the fraction of the total gamma-ray yield attributable to protons of energy less than 23 MeV, assuming power law spectra. For example, for $s=3$, about 98% of the yield of 4.44-MeV gamma rays from the ^{12}C$(p,p')^{12}$C reaction is attributable to protons of energies below 23 MeV.

The absolute magnitudes of the average cross sections presented in Table IV are very sensitive to both the spectral index s and the choice of cutoff energy, E_c, and they are relevant only if the actual proton energy spectrum is close to a power law spectrum. Another perspective on the average cross sections at low proton energies may be obtained from a simple unweighted average, of the form

$$\langle\sigma\rangle=E_m^{-1}\int_0^{E_m}\sigma(E)dE. \tag{4}$$

This average is presented in the last column of Table IV, for the interval from zero to $E_m=20$ MeV.

V. DISCUSSION

Analysis of the gamma-ray line spectrum from an astronomical site can be used to provide detailed information concerning the environment of the site. Extraction of this information may in some cases involve a global analysis: comparing the observed yields of many lines to the predictions of an astrophysical model in which the contributions of all interacting particles are considered. Consideration of the contributions from proton induced reactions provides a major part of the necessary information, but the alpha-particle contribution cannot be ignored. Cross sections for

TABLE IV. Average cross sections (in mb) for the production of gamma rays in proton-induced reactions.

Target nucleus	Residual nucleus	E_γ (MeV)	Beta decay included?[a]	Cross section (mb) Power law spectra[b] $s=2$	$s=3$	$s=4$	Flat spectrum[c]
^{12}C	^{12}C	4.44	Yes	58	23.4	8.2	154
^{16}O	^{12}C	4.44	NA[d]	10	1.6	0.2	20
^{14}N	^{14}N	1.63	Yes	12	5.8	2.3	26
^{14}N	^{14}N	2.31	Yes	21	10.2	4.4	44
^{16}O	^{16}O	6.13	NA	20	6.3	1.7	68
^{20}Ne	^{16}O	6.13	NA	7	1.2	0.2	20
^{20}Ne	^{20}Ne	1.63	Yes	181	142.4	111.4	245
^{24}Mg	^{20}Ne	1.63	NA	11	1.7	0.2	14
^{24}Mg	^{24}Mg	1.37	Yes	174	97.8	51.8	339
^{28}Si	^{28}Si	1.78	Yes	117	62.5	32.4	255
^{56}Fe	^{55}Fe	0.931	No	17	2.6	0.3	30
^{56}Fe	^{55}Fe	0.931	Yes	20	3.0	0.4	34
^{56}Fe	^{55}Fe	1.317	No	12	1.9	0.2	19
^{56}Fe	^{56}Fe	0.847	No	114	53.4	22.8	276
^{56}Fe	^{56}Fe	0.847	Yes	174	76.9	30.4	458
^{56}Fe	^{56}Fe	1.238	No	28	9.7	3.0	96
^{56}Fe	^{56}Fe	1.238	Yes	69	25.4	8.0	218
^{56}Fe	^{56}Fe	1.811	No	12	5.2	1.9	30
^{56}Fe	^{56}Co	0.812	NA	17	6.6	2.1	46

[a] Inclusion of beta decay gives contribution from (p,n) or $(p,2n)$ reactions.
[b] Average cross section calculated from Eq. (3), with $E_c=2$ MeV.
[c] Average cross section calculated from Eq. (4).
[d] Not applicable.

TABLE V. Fraction of gamma-ray yield from reactions at $E \leq 23$ MeV assuming power law spectrum.

Target nucleus	Residual nucleus	E_γ (MeV)	Beta decay included?[a]	Fraction $s=2$	$s=3$	$s=4$
^{12}C	^{12}C	4.44	Yes	0.93	0.98	0.99
^{16}O	^{12}C	4.44	NA[b]	0.44	0.57	0.67
^{14}N	^{14}N	1.63	Yes	0.98	0.99	1.00
^{14}N	^{14}N	2.31	Yes	0.97	0.99	1.00
^{16}O	^{16}O	6.13	NA	0.88	0.96	0.98
^{20}Ne	^{16}O	6.13	NA	0.54	0.68	0.77
^{20}Ne	^{20}Ne	1.63	Yes	0.97	1.00	1.00
^{24}Mg	^{20}Ne	1.63	NA	0.33	0.45	0.56
^{24}Mg	^{24}Mg	1.37	Yes	0.95	0.99	1.00
^{28}Si	^{28}Si	1.78	Yes	0.95	0.99	1.00
^{56}Fe	^{55}Fe	0.931	No	0.40	0.53	0.64
^{56}Fe	^{55}Fe	0.931	Yes	0.39	0.52	0.63
^{56}Fe	^{55}Fe	1.317	No	0.39	0.51	0.61
^{56}Fe	^{56}Fe	0.847	No	0.95	0.99	1.00
^{56}Fe	^{56}Fe	0.847	Yes	0.96	0.99	1.00
^{56}Fe	^{56}Fe	1.238	No	0.92	0.97	0.99
^{56}Fe	^{56}Fe	1.238	Yes	0.95	0.98	1.00
^{56}Fe	^{56}Fe	1.811	No	0.90	0.98	0.99
^{56}Fe	^{56}Co	0.812	NA	0.98	0.99	1.00

[a] Inclusion of beta decay gives contribution from (p,n) or $(p,2n)$ reactions.
[b] Not applicable

alpha-particle induced reactions will be presented in a later paper. Pending these results, we present here a preliminary description of the sort of information which, in principle, can be extracted. (It is to be noted that our caveat about the need for the alpha-particle data may in some cases be too conservative; the Doppler shift for the alpha-particle induced reactions is larger than that for proton-induced reactions and it may therefore be possible in some cases to distinguish between the two contributions, if detectors of good energy resolution are used.)

A commonly used form for the energy spectrum is the power law distribution given by Eq. (2), described by two parameters s (the exponent) and E_c (the cutoff energy). When two or more gamma-ray lines are observed from the same target nucleus, but the energy dependence of the cross section is different, we can determine the shape of the energy spectrum of the accelerated particles, independent of the absolute numbers of particles. An example is given by the $p + {}^{56}Fe$ reaction. The strongest (p,p') gamma rays, at 0.847- and 1.238-MeV, are also strongly excited by (α,α'). However, for three prominent lines the proton cross sections below 23 MeV are large compared

to the alpha particle cross sections: the 0.812-MeV line from the ^{56}Fe(p,n)^{56}Co reaction and the 0.931- and 1.317-MeV lines from ^{56}Fe(p,pn)^{55}Fe. The ratio of either the 0.931- or 1.317-MeV line intensity to that of the 0.812-MeV line can thus give information on the energy spectrum of the accelerated protons, with only a small correction for the alpha-particle contribution. In Fig. 14 we show the ratio of the 0.931- to 0.812-MeV line intensity as a function of the power law exponent s, taking $E_c = 2$ MeV, as above. It is clear that for harder spectra (s smaller) the 0.931-MeV line is relatively more prominent. A similar comparison can be made for the ^{12}C(p,p')^{12}C reactions using the 4.44- and 15.1-MeV lines. The latter line is not observed in the present work but is prominent at higher proton bombarding energies.[32]

When the excitation functions for two gamma rays from two different target nuclei are similar, the ratio of observed yields might be used to determine the relative abundances of these target nuclei in an astrophysical environment, independent of the energy spectrum of the bombarding particles. It is found, for example (ignoring spallation yields and alpha-particle-induced yields), that the ratio of 1.37-MeV gamma rays from $p + ^{24}$Mg to the number of 1.78-MeV gamma rays from $p + ^{28}$Si has little dependence on the parameters E_c and s for a power law distribution; the ratio of ^{24}Mg to ^{28}Si nuclei may thus be measured. Other examples of gamma-ray yield ratios relatively independent of energy spectrum parameters are the ratios of 1.238- or 0.812-MeV gamma rays from ^{56}Fe to 4.44-MeV gamma rays from ^{12}C and the ratio of 0.847-MeV gamma rays from ^{56}Fe to 2.31-MeV gamma rays from ^{14}N. Of course, if some knowledge of the character of the proton spectrum can be obtained, for example, by the comparisons discussed in the previous paragraph or from the widths of the observed gamma-ray lines, then the extraction of relative abundance information will be facilitated.

It is also possible to study the time history of the emission process from line ratios, when there is an appreciable contribution from delayed emissions, as in the case of the ^{56}Co ($t_{1/2} = 78.8$ d) contribution to the ^{56}Fe lines. Consider, in particular, the 1.238- and 0.847-MeV lines from ^{56}Fe. For the ^{56}Co decay, the ratio of these lines is 0.67, while for (p,p') reactions the 1.238-MeV line is relatively much weaker. Thus a ratio of 0.67 would imply remnant activity, a very low ratio would imply an outburst of short duration, and an intermediate ratio would imply a steady state. More quantitative conclusions are dependent on the detailed shape of the proton spectrum.

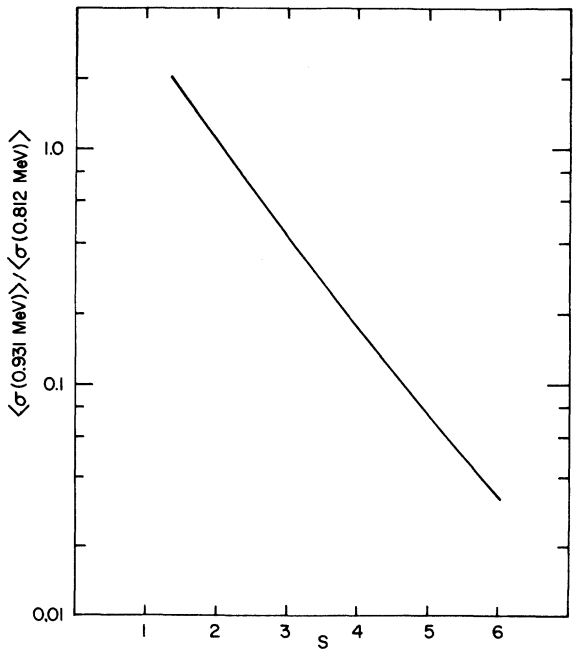

FIG. 14. Ratio of the 0.931-MeV gamma ray yield to the 0.812-MeV gamma ray yield in proton bombardment of ^{56}Fe, where the energy distribution of accelerated protons is assumed to be given by a power law spectrum E^{-s}. The ratio is independent of the cutoff energy E_c, if E_c is less than the threshold energies for both reactions.

It must be recognized that the present observational situation with respect to gamma-ray lines leaves us still a long distance from the detailed analyses considered here. The use to which detailed information on gamma-ray production cross sections can ultimately be put will depend upon the extent to which the hope of obtaining richer and less ambiguous spectra is fulfilled, as the duration of observations is increased and the size and resolution of the detectors is increased.

ACKNOWLEDGMENTS

We wish to thank J. L. Osborne for writing the interactive program used to extract yields from the spectra and E. G. Adelberger and D. Chiang for help in the early stages of the experiment. We also appreciate the aid in data analysis provided by D. Chamberlin and D. Gordon. This work was supported in part by the U. S. Department of Energy and by the National Science Foundation under Grant No. PHY 78-22696.

*Present address.
[1]R. Ramaty, B. Kozlovsky, and R. E. Lingenfelter, Astrophys. J. Suppl. Ser. 40, 487 (1979).
[2]R. E. Lingenfelter and R. Ramaty, Phys. Today 31, No. 3, p. 40 (1978).
[3]NASA Technical Memorandum Report No. 79619, edited by T. L. Cline and R. Ramaty, 1978.
[4]E. L. Chupp, Ref. 3, p. 42.
[5]E. L. Chupp, D. J. Forrest, P. R. Higbie, A. N. Suri, C. Tsai, and P. P. Dunphy, Nature 241, 333 (1973); H. S. Hudson, T Bai, D. E. Gruber, J. L. Matteson, P. L Nolan, and L. E Peterson, Astrophys. J. 236, L91 (1980).
[6]R. C. Haymes, G. D. Walraven, C. A. Meegan, R. D. Hall, F. T. Djuth, and D. H. Shelton, Astrophys. J. 201, 593 (1975).
[7]R. D. Hall, C. A Meegan, G. D. Walraven, F. T. Djuth, and R. C. Haymes, Astrophys. J. 210, 631 (1976).
[8]K. W. Kemper, J. D. Fox, and D. W. Oliver, Phys. Rev. C 5, 1257 (1972), for ^{28}Si.
[9]W. W. Daehnick, Phys. Rev. B 135, 1168 (1964).
[10]R. M Steffen and K. Alder, *The Electromagnetic Interaction in Nuclear Spectroscopy*, edited by W. D. Hamilton (North-Holland, Amsterdam, 1975), p. 505.
[11]A. J. Ferguson, *Angular Correlation Methods in Gamma-Ray Spectroscopy* (North-Holland, Amsterdam, 1965), p. 35.
[12]W. W. Daehnick and R. Sherr, Phys. Rev B 133, 934 (1964).
[13]F. Ajzenberg-Selove, Nucl. Phys A268, 1 (1976).
[14]Hsin-Min Kuan and J. R. Risser, Nucl. Phys. 51, 518 (1964).
[15]A. Richter and L. J. Parish, Phys. Rev. Lett. 21, 1824 (1968).
[16]P. N. Shrivastava, F. Boreli, and B. B. Kinsey, Phys. Rev. 169, 842 (1968).
[17]L. F. Hansen, S. M. Grimes, J. L. Kammerdiener, and V. A. Madsen, Phys. Rev. C 8, 2072 (1973).
[18]R. L. Auble, Nucl. Data Sheets 20, 253 (1977).
[19]Shigeo Tanaka and Michiaki Furukawa, J. Phys. Soc. Jpn. 14, 1269 (1959).
[20]I. L. Jenkins and A. G. Wain, J. Inorg. Nucl. Chem. 32, 1419 (1970).
[21]I. R. Williams and C. B. Fulmer, Phys. Rev. 162, 1055 (1967).
[22]R. L. Brodzinski, L. A. Rancitelli, J. A. Cooper, and N. A. Wogman, Phys. Rev. C 4, 1257 (1971).
[23]W. Zobel, F. C. Maienschein, J. H. Todd, and G. T. Chapman, Nucl. Sci. Eng. 32, 392 (1968).
[24]C. C. Chang, N. S. Wall, and Z. Fraenkel, Phys. Rev. Lett. 33, 1493 (1974).
[25]G. W. Phillips, Patrick Richard, D. O. Elliot, F. F. Hopkins, and A. C. Porter, Phys. Rev. C 5, 297 (1972).
[26]See E. K. Warburton and H. O. Funsten, Phys. Rev. 128, 1810 (1962) and D. K. Scott *et al.*, Nucl. Phys. A99, 177, (1967) for cross sections for scattering to the 12.71- and 15.11-MeV states, and F. D. Reisman *et al.*, Nucl. Phys. A153, 244 (1970) for branching ratios to the ground state.
[27]A. C. L. Barnard, J. B. Swint, and T. B. Clegg, Nucl. Phys. 86, 130 (1966).
[28]J. B. Swint, J. S. Duval, Jr., A. C. L. Barnard, and T. B. Clegg, Nucl Phys. A93, 177 (1967).
[29]Homer E. Conzett, Phys. Rev. 105, 1324 (1957).
[30]J. Kirk Dickens, David A. Haner, and Charles N. Waddell, Phys. Rev. 132, 2159 (1963).
[31]R. L. Dangle, L. D. Oppliger, and G. Hardie, Phys. Rev. B 133, 647 (1964).
[32]J. R. Lapides, C. J. Crannell, H. Crannell, W. F. Hornyak, S. M. Seltzer, J. I. Trombka, and N. S. Wall, Ref. 3, p. 502.